Japanese Journal of Applied Physics

The Japan Society of Applied Physics

REGULAR PAPER

Composition dependence of structural and optical properties in epitaxial $Sr(Sn_{1-x}Ti_x)O_3$ films

To cite this article: Qinzhuang Liu *et al* 2015 *Jpn. J. Appl. Phys.* **54** 031101

Japanese Journal of Applied Physics **54**, 031101 (2015) **REGULAR PAPER**
http://dx.doi.org/10.7567/JJAP.54.031101

Composition dependence of structural and optical properties in epitaxial $Sr(Sn_{1-x}Ti_x)O_3$ films

Qinzhuang Liu[1], Bing Li[1], Hong Li[1]*, Kai Dai[1], Guangping Zhu[1], Wei Wang[1], Yongxing Zhang[1], Guanyin Gao[2], and Jianming Dai[3]

[1]*School of Physics and Electronic Information, Huaibei Normal University, Huaibei 235000, P. R. China*
[2]*Hefei National Laboratory for Physical Sciences at Microscale, University of Science and Technology of China, Hefei, 230029, P. R. China*
[3]*Institute of Solid State Physics, Chinese Academy of Science, Hefei 230031, P. R. China*
E-mail: lihonggreat@126.com

Received September 11, 2014; accepted December 4, 2014; published online February 5, 2015

Epitaxial $Sr(Sn_{1-x}Ti_x)O_3$ (SSTO, $x = 0$–1) thin films were grown on MgO substrates by a pulsed laser deposition technique. The effects of composition on the structural and optical properties of SSTO films were investigated. X-ray diffraction studies show that the lattice parameter decreases from 4.041 to 3.919 Å gradually with increasing Ti content from 0 to 1 in SSTO films. Optical spectra analysis reveals that the band gap energy E_g decreases continuously from 4.44 to 3.78 eV over the entire doping range, which is explained by the decreasing degree of octahedral tilting distortion and thus the increasing tolerance factor caused by the increasing small-Ti-ion doping concentration.

1. Introduction

Achieving wide-range tuning of the band gap in semiconductors has attracted much attention recently owing to the impetus of optoelectronic device applications and material research, such as solar cells, band gap-tailored heterostructures, and transparent conducting materials.[1–4] Particularly for the ABO_3 perovskite-structured materials, apart from their remarkable physical properties, their structures composed of off-centered cations and corner-sharing BO_6 octahedra are tolerant to lattice distortion, which allows a wide range of internal distortions associated with rotations of the octahedra. Thus a large and controllable band-gap tuning can be easily achieved to fulfill the requirement for more efficient transparent conducting oxide and solar energy conversion applications in a perovskite-type oxide solid solution between different perovskite-structured materials or by substituting with other elements. For example, for $LaCoO_3$-alloyed $Bi_4Ti_3O_{12}$, the band gap was reduced by as much as ~1 eV by site-special substitutional alloying.[1] The $SrTi_{1-x}Fe_xO_3$ solid-solution system exhibited a systematic band-gap decrease of 1.8 eV across the entire composition range.[5] For the $BaTiO_3$–$BaZrO_3$ solid-solution system, the band gap was tuned continuously from 2.92 to 3.84 eV.[6]

More recently, wide-band-gap perovskite-type stannates, with the general chemical formula $RSnO_3$ (R = Ba, Sr, and Ca), have gained considerable attention owing to their particular and interesting physical properties when doped with many other elements, as well as potential applications in humidity sensors, thermal stable capacitors and so forth.[7–12] Among the compounds $RSnO_3$, $SrSnO_3$ has a wide band gap of 4.27 eV and an orthorhombic $GdFeO_3$-type structure with lattice parameters of $a = 5.709$ Å, $b = 5.703$ Å, and $c = 8.065$ Å.[13] Pure $SrSnO_3$ can be used in capacitors as a dielectric material and an insulating buffer layer for heterostructures, and in gas sensors. Moreover, doped $SrSnO_3$ was observed to show a marked diversity of physical properties, including transparent conducting characteristics with La or Sb doping,[14–17] half-metallic ferromagnetism with Fe doping,[18] and an intense green luminescence induced by Tb–Mg codoping.[19]

On the other hand, $SrTiO_3$ is a well-known perovskite-type insulator with the space group $Pm3m$ and a wide band gap of about of 3.2 eV.[20] It has attracted considerable scientific and technological interest owing to its various physical and chemical properties. Although the $SrSnO_3$ and $SrTiO_3$ have been intensively investigated respectively, Ti-doped $SrSnO_3$ [$Sr(Sn_{1-x}Ti_x)O_3$], the solid solution between these two wide-band gap perovskite-type oxides was not probed intensively. Previous studies were only limited to the synthesis of $Sr(Sn_{1-x}Ti_x)O_3$ bulk ceramics and the analysis of their electrical, dielectric, and thermal behaviors.[21–24] In this paper, we report on $Sr(Sn_{1-x}Ti_x)O_3$ (SSTO) films with $x = 0$–1 grown on MgO(001) substrates by pulsed laser deposition (PLD). The effects of composition on the structural and optical properties of SSTO films were investigated in detail, and the wide-range tuning of the band gap was achieved.

2. Experimental procedure

$Sr(Sn_{1-x}Ti_x)O_3$ ($x = 0$, 0.20, 0.40, 0.60, 0.80, and 1) ceramic targets were prepared by high-temperature solid reactions using raw materials of $SrCO_3$ (99.5% in purity), SnO_2 (99.5% in purity), and TiO_2 (99.99% in purity) (Sinopharm Chemical Reagent). After grounding and presintering twice, the powders were pressed to form disks and sintered at 1450 °C for 24 h, and then cooled to room temperature at a rate of 5 °C/min. Thin films of SSTO were epitaxially grown on MgO(00l) single-crystalline substrates by PLD using a 248 nm KrF excimer laser. The substrate-to-target spacing was 5.5 cm and laser energy density was about 1.6 J/cm^2. During deposition, the oxygen pressure and the substrate temperature were kept at 20 Pa and 740 °C respectively for all the samples. After deposition, the films were annealed in situ for about 10 min under the same temperature and oxygen pressure as those in the case of deposition before cooling. The film thickness was determined to be 260 ± 10 nm by cross-sectional field-emission scanning electron microscopy. The chemical composition of the films was assumed to be the same as that of the targets. The SSTO film structures were characterized by X-ray diffraction (XRD) using Cu Kα_1 radiation with $\lambda = 1.5406$ Å (Philips X'pert). Surface morphologies were examined by tapping-mode atomic force microscopy (AFM; Veeco Multimode V). The optical transmission and reflection spectra of the SSTO films were measured with a conventional spectrophotometer (Hitachi U-4100) in the wavelength range of 200–2000 nm.

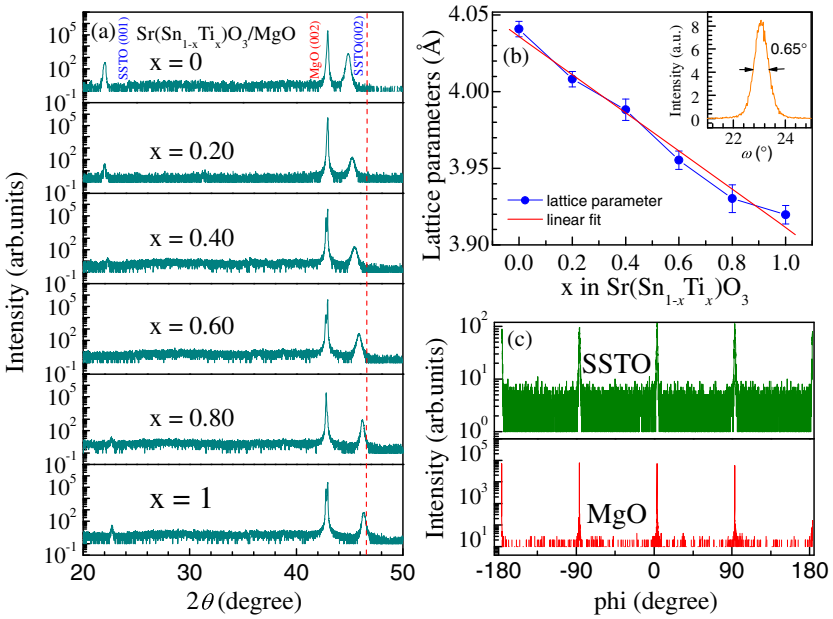

Fig. 1. (Color online) (a) XRD linear scan spectra from SSTO films with Ti doping concentrations ranging from $x = 0$ to 1. Dashed lines serve as visual guides. (b) Out-of-plane lattice parameters of SSTO films as a function of Ti concentration x. Error bars represent the standard deviation calculated based on XRD (00l) peak position. The inset shows a typical ω-scan rocking curve from the SSTO(002) peak. (c) φ scan pattern of both the SSTO films and the MgO substrate around (202) reflections.

3. Results and discussion

Figure 1(a) shows the X-ray θ–2θ linear scan spectra from the SSTO films grown on MgO(001) substrates. Only the diffraction peaks from the (00l) planes of the SSTO films and MgO substrates appeared in the scans, and no diffraction peaks from secondary phases or randomly oriented grains were observed, indicating that the films exhibit a preferred orientation along the c-axis of the perovskite structure. As can be seen from Fig. 1(a), with increasing Ti doping concentration from 0 to 1, the location of the SSTO (00l) reflection peak moves gradually towards the high-angle direction. Then out-of-plane lattice parameters are obtained from XRD linear scans with values decreasing linearly from $c = 4.041$ Å of $SrSnO_3$ at $x = 0$ to $c = 3.919$ Å of $SrTiO_3$ at $x = 1$, as shown in Fig. 1(b). The variations between the composition x and the lattice parameter (c-axis) are consistent with Vegard's law.[25] The equation $c = 4.036 - 0.125x$ was obtained by linear fitting of the out-of-plane lattice parameters of the SSTO films. A similar phenomenon was also observed in $Ba_{1-x}Sr_xSnO_3$ and $Ba(Ti_{1-x}Sn_x)O_3$ solid solutions.[26,27] The decrease in lattice constant is due to the substitution of large-ionic-radius Sn^{4+} ($R_{ef} = 0.69$ Å) by a small-ionic-radius Ti^{4+} ($R_{ef} = 0.605$ Å),[22,28] which indicates that Ti^{4+} ions were dissolved in the $SrSnO_3$ lattice in the entire doping range. The full widths at half maximum of the X-ray rocking curves at the (002) reflections of the SSTO films are in the range of 0.60–0.90°, as shown in the inset of Fig. 1(b). To determine the epitaxial relationship between the films and the substrates, XRD Φ scans were measured on SSTO(202) and MgO(202) reflections at a scanning rate of 6°/min and a scanning step of 0.02°. A representative scan of SSTO at $x = 0.04$ is shown in Fig. 1(c). A set of four distinct peaks with 90° spacing indicates that the SSTO films were grown on MgO(001) substrates with the cube-on-cube epitaxial relationship.

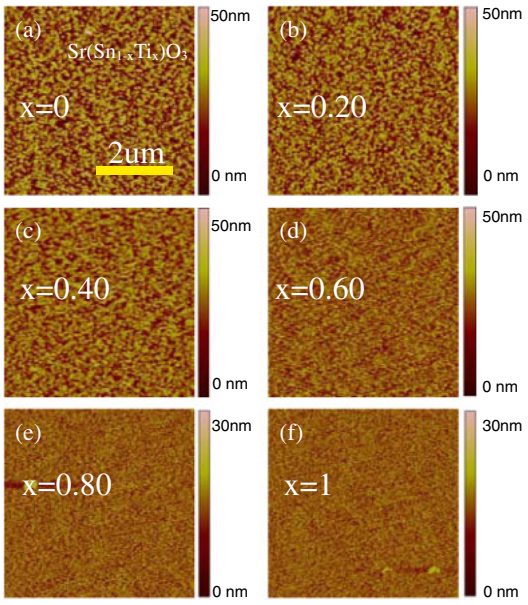

Fig. 2. (Color online) AFM images of SSTO thin films deposited at MgO(001) substrates with Ti doping concentrations of (a) $x = 0$, (b) $x = 0.20$, (c) $x = 0.40$, (d) $x = 0.60$, (e) $x = 0.80$, and (f) $x = 1$.

Figures 2(a)–2(f) show the surface morphologies of SSTO films with Ti concentrations ranging from $x = 0$ to 1 investigated by AFM with a scanning area of $5 \times 5\,\mu m^2$. The root-mean-square surface roughnesses are 8.10, 6.83, 5.33, 4.82, 3.02, and 2.68 nm for SSTO films at $x = 0$, 0.20, 0.40, 0.60, 0.80, and 1, suggesting that the film surfaces become smoother gradually with increasing Ti concentration in the SSTO films.

Figure 3(a) shows the transmittance and reflection spectra of the SSTO/MgO(001) heterostructures in the wavelength

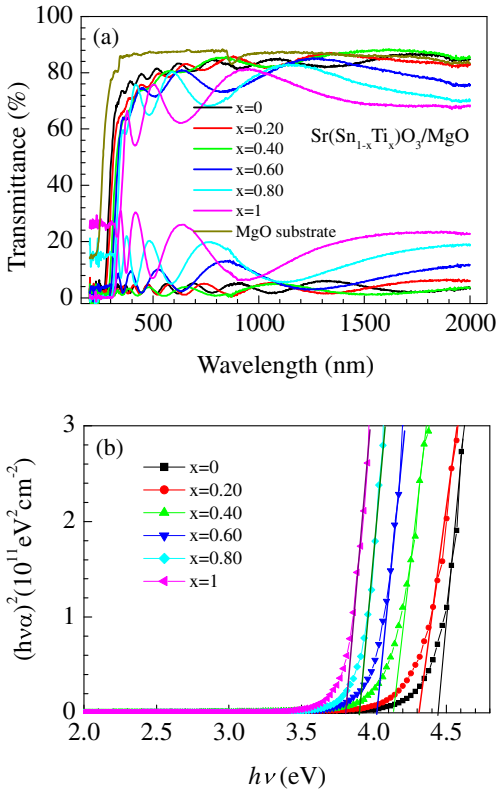

Fig. 3. (Color online) (a) Optical transmission and reflection spectra of SSTO thin films at different Ti concentrations, and pure MgO substrate for comparison. (b) $(h\nu\alpha)^2$ versus $h\nu$ plots of SSTO thin films.

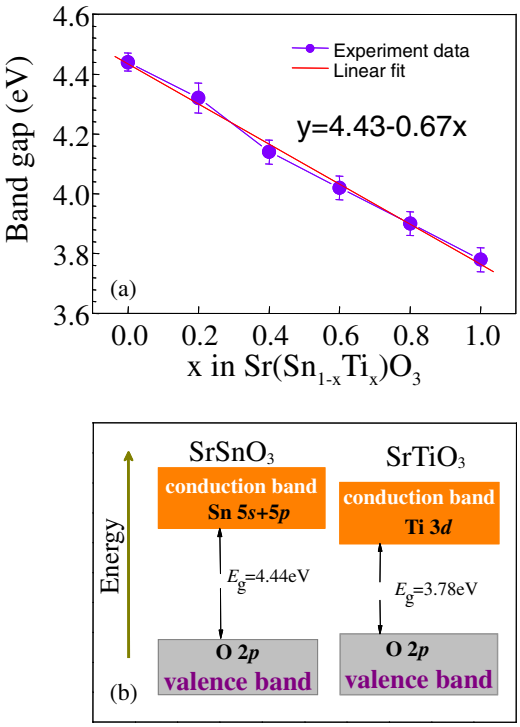

Fig. 4. (Color online) (a) Optical band gaps variation as a function of Ti concentration in SSTO films. Error bar originates from the uncertainty in the extrapolation of the absorption curves down to the base line. The solid line is the linear fitting to the experimental data. (b) Electric structures for SSTO films at low Ti concentration of $x = 0$ and high Ti concentration of $x = 1$ with band-gap energies of 4.44 and 3.78 eV, respectively.

range of 200–2000 nm, and those of the bare MgO(001) substrate were also given for comparison. It is observed that all the SSTO films have a high transparency of more than 85% in the visible and near-infrared ranges. The oscillations of the spectra are caused by the optical interference at the interface between the films and the substrates. More interestingly, the transmittance spectra of SSTO films show a sharp optical absorption edge in the ultraviolet region, which corresponds to the band gaps of the SSTO films. Moreover, the edge shifts gradually towards longer wavelength sides with increasing Ti doping concentration in the films. The optical absorption coefficient α can be calculated from the well-known relation, $\alpha = (1/d)\ln[(1-R)/T]$, where T is the transmittance, R is the reflectance, and d is the thickness of the films. The optical band gap E_g of the SSTO films can be obtained by using α with the equation

$$(h\nu\alpha)^2 = A(h\nu - E_g), \tag{1}$$

where A is a constant, and $h\nu$ is the incident photon energy. Figure 3(b) shows the $(h\nu\alpha)^2$ versus $h\nu$ plot and E_g was estimated by extrapolating the linear portion against the photon energy. It was found that the calculated band gaps of the SSTO films are strongly dependent on the composition. With increasing Ti concentration in the films, E_g decreases continuously from 4.44 to 3.78 eV. In comparison, for the Ti-doped films at $x = 1$, namely, $SrTiO_3$ films, the calculated band gap of 3.78 eV is slightly higher than those of 3.73 eV reported by Soledade et al.[29] and 3.58 eV reported by Du et al.[28] for the thin films, and that of 3.22 eV for bulk $SrTiO_3$. On the other hand for Ti-doped films at $x = 0$, namely, pure $SrSnO_3$ films, the calculated band gap of 4.44 eV is also higher than that of 4.27 eV reported by Endo et al.[30] and Vegas et al.[31]

Figure 4(a) shows the band-gap energy E_g of SSTO films as a function of the Ti doping concentration. Error bars were estimated from the uncertainty by the extrapolation of absorption curves down to the base line. A near-linear relationship was obtained between the band-gap energy E_g and the Ti concentration x in the system. Over the entire solid solution range, the band-gap energy can be fitted linearly as $E_g(x) = 4.43 - 0.67x$. Eng et al.[32] have reported that the octahedral tilt distortion in perovkite oxides narrows the conduction band and leads to a large increase in band gap. The gradual decrease in the band gap of SSTO films can be explained in terms of the increase in Goldschmidt tolerance factor,[32,33] which is defined by $2^{1/2}(r_B + r_O)t = r_A + r_O$. For the perovskite-structured solid solution $A_{1(1-x)}A_{2x}B_{1(1-x)}B_{2x}O_3$, the tolerance factor can be expressed by[33]

$$t_{ss} = \frac{(1-x)r_{A1} + xr_{A2} + r_O}{\sqrt{2}[(1-y)r_{B1} + yr_{B2} + r_O]} \tag{2}$$

where r_A, r_B, and r_O are the ionic radii of each atom for the perovskite ABO_3 structure. For the SSTO system, the tolerance factor t_{ss} was calculated to be 0.961, 0.969, 0.977, 0.985, 0.993, and 1.001 for Ti doping concentration of at $x = 0$, 0.20, 0.40, 0.60, 0.80, and 1, using ionic radii of $r_{Sr} = 1.44$ Å, $r_{Sn} = 0.69$ Å, $r_{Ti} = 0.605$ Å, and $r_O = 1.40$ Å.[34,35] The deviation of the tolerance factor from unity implies the octahedral tilting of the structure.[34] Band structure and density of state calculations show that, for

the perovskite-structured $SrSnO_3$, the top of the valence band is completely composed of O 2p orbitals, and the bottom of the conduction band consists of Sn 5s orbitals with minor contributions of the Sn 5p states.[7,18,34] However, with increasing Ti concentration in the SSTO system, the tolerance factor increases gradually to unity, suggesting that the degree of the octahedral tilting distortion decreases correspondingly. In this case, the doping Ti 3d states will contribute to the bottom of the conduction band and make the conduction band become wider than that of SSTO films, thereby reducing the band gap correspondingly.[36] As a result, for the film with Ti doping concentration of $x = 1.0$, the oxygen octahedron becomes undistorted, and the band gap decreases to 3.78 eV for the $SrTiO_3$, whose valence band is mainly composed of O 2p orbitals and whose the conduction band consists of Ti 3d orbitals,[20] as shown in Fig. 4(b). Similar phenomena were also observed in other perovskite-structured solid solutions, such as $BaTiO_3$–$CaTiO_3$, $BaTiO_3$–$BaZrO_3$, and $BaSnO_3$–$SrSnO_3$.[6,10]

4. Conclusions

$Sr(Sn_{1-x}Ti_x)O_3$ ($x = 0$–1) films were epitaxially grown on MgO substrates by PLD. X-ray diffraction, atomic force microcopy, and optical transmittance and reflectance investigations reveal that the lattice and band structure properties of the SSTO films can be modified significantly by changing the Ti concentration. With increasing Ti concentration from 0 to 1 in the SSTO films, out-of-plane parameters decrease gradually from 4.041 to 3.919 Å as a result of the substitution of Sn^{4+} ions by Ti^{4+} with a smaller ionic radius. Furthermore, the band-gap energy decreases from 4.44 to 3.78 eV, which can be explained in terms of the decreasing degree of octahedral tilting distortion and thereby the increasing tolerance factor caused by the increasing doping level of smaller Ti ions. The band-gap modulation in a wide energy range suggests that the SSTO films have potential application in solar energy conversion devices.

Acknowledgments

This work was supported by the Chinese Natural Science Foundation (Nos. 11004071, 11374304, and 51302101), Natural Science Foundation of Anhui Province (No. 1408085QA19), and Huaibei Scientific Talent Development Scheme (No. 20130304).

1) W. S. Choi, M. F. Chisholm, D. J. Singh, T. Choi, G. E. Jellison, Jr., and H. N. Lee, Nat. Commun. **3**, 689 (2012).
2) T. Choi, S. Lee, Y. J. Choi, V. Kiryukhin, and S. W. Cheong, Science **324**, 63 (2009).
3) J. W. Bennett, I. Grinberg, and A. M. Rappe, J. Am. Chem. Soc. **130**, 17409 (2008).
4) S. Y. Yang, J. Seidel, S. J. Byrnes, P. Shafer, C. H. Yang, M. D. Rossel, P. Yu, Y. H. Chu, J. F. Scott, J. W. Ager, L. W. Martin, and R. Ramesh, Nat. Nanotechnol. **5**, 143 (2010).
5) A. Rothschild, W. Menesklou, H. L. Tuller, and E. Ivers-Tiffée, Chem. Mater. **18**, 3651 (2006).
6) S. Lee, R. D. Levi, W. Qu, S. C. Lee, and C. A. Randall, J. Appl. Phys. **107**, 023523 (2010).
7) D. J. Singh, Q. Xu, and K. P. Ong, Appl. Phys. Lett. **104**, 011910 (2014).
8) H. R. Liu, J. H. Yang, H. J. Xiang, X. G. Gong, and S. H. Wei, Appl. Phys. Lett. **102**, 112109 (2013).
9) H. J. Kim, U. Kim, H. M. Kim, T. H. Kim, H. S. Mun, B. G. Jeon, K. T. Hong, W. J. Lee, C. Ju, K. H. Kim, and K. Char, Appl. Phys. Express **5**, 061102 (2012).
10) H. Mizoguchi, P. M. Woodward, C. Park, and D. A. Keszler, J. Am. Chem. Soc. **126**, 9796 (2004).
11) Y. P. Yuan, J. Lv, X. J. Jiang, Z. S. Li, T. Yu, Z. G. Zou, and J. H. Ye, Appl. Phys. Lett. **91**, 094107 (2007).
12) P. H. Borse, U. A. Joshi, S. M. Ji, J. S. Jang, J. S. Lee, E. D. Jeong, and H. G. Kim, Appl. Phys. Lett. **90**, 034103 (2007).
13) M. A. Green, K. Prassides, P. Day, and D. A. Neumann, Int. J. Inorg. Mater. **2**, 35 (2000).
14) Q. Z. Liu, J. J. Liu, B. Li, H. Li, G. P. Zhu, K. Dai, Z. L. Liu, P. Zhang, and J. M. Dai, Appl. Phys. Lett. **101**, 241901 (2012).
15) X. Luo, Y. S. Oh, A. Sirenko, P. Gao, T. A. Tyson, K. Char, and S. W. Cheong, Appl. Phys. Lett. **100**, 172112 (2012).
16) Q. Liu, J. Dai, Z. Liu, X. Zhang, G. Zhu, and G. Ding, J. Phys. D **43**, 455401 (2010).
17) H. J. Kim, J. Kim, T. H. Kim, W. J. Lee, B. G. Jeon, J. Y. Park, W. S. Choi, D. W. Jeong, S. H. Lee, J. Yu, T. W. Noh, and K. H. Kim, Phys. Rev. B **88**, 125204 (2013).
18) I. R. Shein, V. L. Kozhevnikov, and A. L. Ivanovskii, Semiconductors **40**, 1261 (2006).
19) K. Ueda, T. Yamashita, K. Nakayashiki, K. Goto, T. Maeda, K. Furui, K. Ozaki, Y. Nakachi, S. Nakamura, M. Fujisawa, and T. Miyazaki, Jpn. J. Appl. Phys. **45**, 6981 (2006).
20) N. Shanthi and D. D. Sarma, Phys. Rev. B **57**, 2153 (1998).
21) A. L. M. de Oliveira, M. R. S. Silva, H. Sales, E. Longo, A. S. Maia, A. G. Souza, and I. M. G. Santos, J. Therm. Anal. Calorimetry **114**, 565 (2013).
22) A. Stanulis, A. Selskis, R. Ramanauskas, A. Beganskiene, and A. Kareiva, Mater. Chem. Phys. **130**, 1246 (2011).
23) S. Singh, P. Singh, O. Parkash, and D. Kumar, Adv. Appl. Ceram. **106**, 231 (2007).
24) L. Wu, C. C. Wu, and M. M. Wu, J. Electron. Mater. **19**, 197 (1990).
25) L. Vegard, Z. Phys. **5**, 17 (1921) [in German].
26) B. Ramdas and R. Vijayaraghavan, Bull. Mater. Sci. **33**, 75 (2010).
27) J. W. Zhai, B. Shen, X. Yao, L. Y. Zhang, and H. Chen, J. Am. Ceram. Soc. **87**, 2223 (2004).
28) F. Du, B. Cui, H. Cheng, R. Niu, and Z. Chang, Mater. Res. Bull. **44**, 1930 (2009).
29) L. E. B. Soledade, E. Longo, E. R. Leite, F. M. Pontes, F. Lanciotti, Jr., C. E. M. Campos, P. S. Pizani, and J. A. Varela, Appl. Phys. A **75**, 629 (2002).
30) T. Endo, T. Matsuda, H. Takizana, and M. Shimada, J. Mater. Sci. Lett. **11**, 1330 (1992).
31) A. Vegas, M. Vallet-Regi, J. M. Gonzalez-Calbet, and M. A. Alario-Franco, Acta Crystallogr., Sect. B **42**, 167 (1986).
32) H. W. Eng, P. W. Barnes, B. M. Auer, and P. M. Woodward, J. Solid State Chem. **175**, 94 (2003).
33) S. Lee, W. H. Woodford, and C. A. Randall, Appl. Phys. Lett. **92**, 201909 (2008).
34) W. F. Zhang, J. W. Tang, and J. H. Ye, J. Mater. Res. **22**, 1859 (2007).
35) S. Singh, P. Singh, C. R. Gautam, O. Parkash, and D. Kumar, Int. Symp. Research Students on Material Science and Engineering, 2004.
36) P. H. Borse, J. S. Lee, and H. G. Kim, J. Appl. Phys. **100**, 124915 (2006).